Journal of Solid State Chemistry **151,** 46–55 (2000)
doi:10.1006/jssc.2000.8620, available online at http://www.idealibrary.com on IDEAL®

Crystal Structure and Properties of $Nd_4Co_3O_{10+\delta}$ and $Nd_4Ni_3O_{10-\delta}$

Anja Olafsen,* Helmer Fjellvåg,[1,*] and Bjørn C. Hauback†

*Department of Chemistry, University of Oslo, P.O. Box 1033 Blindern, N-0315 Oslo, Norway; and †Institute for Energy Technology, N-2027 Kjeller, Norway

Received August 24, 1999; in revised form December 22, 1999; accepted January 10, 2000

The crystal structures of $Nd_4M_3O_{10}$ (M = Co, Ni) correspond to the $n = 3$ members of the Ruddlesden–Popper series of $A_{n+1}B_nO_{3n+1}$. Rietveld-type analyses of high-resolution powder synchrotron X-ray and powder neutron diffraction (PND) data of $Nd_4Co_3O_{10+\delta}$ and $Nd_4Ni_3O_{10-\delta}$ reveal their crystal structures to be slightly monoclinically distorted. The symmetry lowering to space group $P2_1/a$ is caused by tilting of the MO_6 octahedra within the $(NdMO_3)_3$ layers. Long apical M–O distances are observed in the octahedra pointing toward the NdO layers. Magnetic susceptibility data for $Nd_4Co_3O_{10.00}$ indicate long-range antiferromagnetic ordering below 15 K. The ordered moment is too low to be detected by PND at 8 K. Above 60 K, two nearly Curie–Weiss paramagnetic regions are observed: 60–560 K and 650–920 K. Thermal analysis data for $Nd_4Co_3O_{10+\delta}$ in atmospheres of oxygen and nitrogen shows a complex behavior, with respect to both possible phase transitions and redox properties. © 2000 Academic Press

Key Words: **Ruddlesden–Popper-type phases; structural properties; magnetic properties; thermal properties.**

INTRODUCTION

The crystal structure of $Ln_4M_3O_{10}$ (Ln = La, Pr, Nd and M = Co, Ni) corresponds to that for the $n = 3$ members in the Ruddlesden–Popper (RP) series of $A_{n+1}B_nO_{3n+1}$ (1). In these compounds, three consecutive perovskite layers $[(LnMO_3)_3]$ alternate with one rock salt LnO layer along the crystallographic c-direction, i.e., $(Ln\text{O})(LnMO_3)_3$. In earlier studies (2–5) these phases were reported to belong to the orthorhombic crystal system with an F-centred unit cell. However, recent investigations performed with electron diffraction (6, 7) and high-resolution synchrotron X-ray diffraction (SXRD) (8) show that the symmetry is lower. Hansteen and Fjellvåg (8) reported that stoichiometric and nonstoichiometric $La_4Co_3O_{10+\delta}$ crystallize in the monoclinic crystal system with space group $C2/m$. However, powder neutron diffraction (PND) data clearly reveal additional reflections not compatible with C-centering, and on that basis Fjellvåg *et al.* (9) showed the correct space group to be $P2_1/a$. The reason for the symmetry lowering is tilting of the MO_6 octahedra within the $(LnMO_3)_3$ triple layers.

The relation between oxygen nonstoichiometry and crystal structure is intriguing in these compounds, in particular on the basis of the multiphase nature of $La_2NiO_{4+\delta}$ (10–15). Furthermore, the complex electronic properties of $LaCoO_3$, $NdCoO_3$, and $LnNiO_3$ (Ln = La, Pr, Nd, Sm) [see e.g. (8, 16, 17)] call for studies on the behavior of the RP-type derivatives, with layer-like perovskite-type structure elements.

The present paper reports on the crystal structures of $Nd_4Co_3O_{10+\delta}$ and $Nd_4Ni_3O_{10-\delta}$ as obtained from refinements of high-resolution SXRD and PND data at 298 K. For $Nd_4Co_3O_{10+\delta}$, which so far has been given little attention in the literature, also oxygen nonstoichiometry, magnetic, and thermal properties are reported.

EXPERIMENTAL

Synthesis

Samples of $Nd_4Co_3O_{10+\delta}$ and $Nd_4Ni_3O_{10-\delta}$ were synthesised on basis of the citric acid method. Starting materials were Nd_2O_3 (99.99%, Molycorp), $Ni(CH_3COO)_2 \cdot 4H_2O$ (>99%, Fluka), $Co(CH_3COO)_2 \cdot 4H_2O$ (>99%, Fluka), citric acid monohydrate, $C_3H_4(OH)(COOH)_3 \cdot H_2O$ (>99.8%, Riedel-de Haën), and HNO_3 (min. 65% for analysis, Riedel-de Haën). Nd_2O_3 was dried at 1273 K for 12 hours prior to use and cooled to room temperature in a desiccator. Exact formula weights of the adopted nickel and cobalt acetates were determined gravimetrically by decomposition of the acetates into NiO and Co_3O_4, respectively, in air at 1073 K overnight.

Nd_2O_3 was dissolved in 4 M HNO_3 at approximately 373 K under stirring conditions before being mixed with a solution of dissolved $Ni/Co(CH_3COO)_2 \cdot 4H_2O$. Thereafter citric acid was added in excess to the solution and the mixture was melted on further heating. Nitrous gas species

[1] To whom correspondence should be addressed. E-mail: helmer.fjellvag@kjemi.uio.no.

0022-4596/00 $35.00

and water were boiled off. The obtained material was dried at 453 K and thereafter calcined at 773 K for 4 hours and at 1073 K for 1 hour. Phase pure samples of $Nd_4Co_3O_{10}$ and $Nd_4Ni_3O_{10}$ were obtained after one or two further annealing steps in a tube furnace, respectively at 1393 K in N_2 and 1248 K in O_2. The oxygen content (δ) of the samples depends strongly on the cooling conditions. For $Nd_4Co_3O_{10+\delta}$, the oxygen contents were determined gravimetrically by subsequent oxidation of the samples in pure oxygen into $NdCoO_3$ and Nd_2O_3 at 1300 K. For example, a sample with $\delta = 0.00$ is obtained on cooling $Nd_4Co_3O_{10+\delta}$ from 1393 K to ambient under a stream of nitrogen and $\delta = 0.20$ is obtained for samples taken out of the furnace at 1393 K and cooled in air. For $Nd_4Ni_3O_{10-\delta}$, $\delta = 0.15$ was obtained on cooling from 1248 K to ambient in a stream of oxygen (6).

Powder Diffraction

The purity of the synthesized samples was ascertained from powder X-ray diffraction (PXD) data collected with Guinier–Hägg cameras using Cr$K\alpha_1$ radiation ($\lambda =$ 228.970 pm). Data for determination of unit cell dimensions were collected on a D5000 diffractometer with Cu$K\alpha_1$ radiation ($\lambda = 154.0598$ pm), a primary monochromator, and a position-sensitive detector (PSD). Si was used as internal standard [$a = 543.088$ pm (18)] and the CELLKANT program (19) was used for refinements of unit cell dimensions.

Synchrotron powder X-ray diffraction (SXRD) data were collected for $Nd_4Co_3O_{10.20}$ at the Swiss Norwegian Beam Line (BM 1) at ESRF, Grenoble, France. Data at 298 K were measured between $2\theta = 9.00$ and 60.00° in steps of $\Delta(2\theta) = 0.007°$ with the powder diffractometer in Debye–Scherrer mode. Monochromatic X-rays with wavelength 110.103 pm were obtained from a channel-cut Si(111) crystal. The sample was kept in a rotating glass capillary with diameter 0.5 mm.

Powder neutron diffraction (PND) data for $Nd_4Co_3O_{10.00}$ (8, 298 K) and $Nd_4Ni_3O_{9.85}$ (298 K) were collected between $2\theta = 10.00$ and 130.00° in steps of $\Delta(2\theta) = 0.05°$ with the two-axis powder diffractometer PUS at the JEEP II reactor, Kjeller, Norway. Monochromatic neutrons with wavelength 155.58 pm were obtained by means of a Ge(511) monochromator. Scattered intensities were measured with two detector units, each containing a vertical stack of seven position-sensitive ^{3}He detectors, all covering 20° in 2θ. The samples were contained in cylindrical sample holders of vanadium, sealed with an indium washer. Low temperatures were obtained by means of a Displex cooling system. A Lake Shore DRC 82C controller was used and the temperature was measured and controlled by use of a silicon diode.

The GSAS program package (20) was used for Rietveld-type refinements of both the SXRD and the PND data. Table 1 summarizes relevant facts for the data sets and the parameters entering the least-squares refinements. Common isotropic displacement factors were adopted for atoms of the same type. In the case of the PND data, the peak shape was modeled using a Gaussian function whereas for the SXRD data a pseudo-Voigt function with three Gaussian and four Lorentzian profile coefficients (two Scherrer and two strain broadening coefficients) was adopted. For the PND data of $Nd_4Ni_3O_{9.85}$ an asymmetric peak shape coefficient was also activated. The background in all data sets was modeled by cosine Fourier series polynomials. In order to model the amorphous contribution from the glass capillary in the SXRD data set of $Nd_4Co_3O_{10.20}$ as many as 33 background coefficients were applied. The neutron scattering lengths $b_{Nd} = 7.69$ fm, $b_{Co} = 2.53$ fm, $b_{Ni} = 10.30$ fm, and $b_O = 5.81$ fm were taken from the GSAS library (20).

TABLE 1
Relevant Features of the Powder Synchrotron X-ray (298 K) and Neutron (8, 298 K) Diffraction Data Sets and the Parameters Entering the Profile Refinements for $Nd_4Co_3O_{10+\delta}$ and $Nd_4Ni_3O_{10-\delta}$

	$Nd_4Co_3O_{10.00}$, 8 K,	$Nd_4Co_3O_{10+\delta}$, 298 K		$Nd_4Ni_3O_{9.85}$, 298 K
	PND	PND, $\delta = 0.00$	SXRD, $\delta = 0.20$	PND
Measured data points	2399	2399	7286	2399
Reflections (*hkl*)	1757	1760	1784	1773
Scale factor	1	1	1	1
Zero point	1	1	1	1
Profile parameters	3	3	7	4
Unit cell dimensions	4	4	4	4
Atomic coordinates	48	48	18	48
Displacement factors	3	3	3	3
Background coefficients	12	12	33	12
Refinable parameters	72	72	67	73

Magnetic Measurements

Magnetic susceptibility data were measured for $Nd_4Co_3O_{10.00}$ in the temperature region 5–320 K with an MPMS system (Quantum Design). The samples were kept in gelatine capsules, cooled in zero field, and measured during heating in a magnetic field of 1000 Oe. A Faraday balance was used when measuring the magnetic susceptibility in the temperature region 290–920 K ($H \leq 7000$ Oe). The samples were kept in sealed, evacuated silica glass capillaries. Calibrations were performed by measurements of standards of Pd (MPMS, from NIST) and $HgCo(SCN)_4$ (Faraday).

Thermal Analysis

Thermogravimetric analysis (TGA) and differential thermal analysis (DTA) of $Nd_4Co_3O_{10.00}$ were respectively performed with a Perkin Elmer TGA7 and a DTA7 system in atmospheres of nitrogen and oxygen in the temperature interval 350–1375 K. The heating rate was $10\ K \cdot min^{-1}$. Standard programs for the systems were used in the data reduction.

RESULTS AND DISCUSSION

The oxygen content of $Nd_4Co_3O_{10+\delta}$ is strongly dependent on the pT conditions, see TGA data in Fig. 1. For $Nd_4Co_3O_{10+\delta}$, samples with oxygen content $\delta = 0.00$ (PND) and $\delta = 0.20$ (SXRD) were selected for crystal structure refinements. The $La_4Co_3O_{10+\delta}$ analogue is reported to exhibit a broad homogeneity region for $0 \leq \delta \leq 0.30$ (8). On the other side, the related $La_2NiO_{4+\delta}$ system shows complex behavior with respect to both nonstoichiometry and polymorphism (10–15). In the case of $Nd_4Co_3O_{10+\delta}$, a careful inspection of the conventional XRD patterns taken at 298 K does not indicate any structural difference between samples with different oxygen contents. The available diffraction data (XRD, SXRD, and PND) for $Nd_4Co_3O_{10+\delta}$ give no clear evidence for any two-phase situation with crystallographically related phases. Hence, in the structure analysis of $Nd_4Co_3O_{10+\delta}$, the samples with the different oxygen contents $\delta = 0.00$ and $\delta = 0.20$ are assumed to relate to the same phase. A more complete discussion of the thermal analysis data is given below.

Crystal Structure

The XRD patterns for $Nd_4Co_3O_{10+\delta}$ and $Nd_4Ni_3O_{9.85}$ at 298 K can be indexed on an F-centered orthorhombic unit cell as described by Seppänen and workers (2, 3) for the $La_4M_3O_{10}$ (M = Ni, Co) analogues. However, present conventional powder X-ray diffractograms showed significant peak broadening for certain Bragg reflections, which is in agreement with reports by other research groups (6, 8).

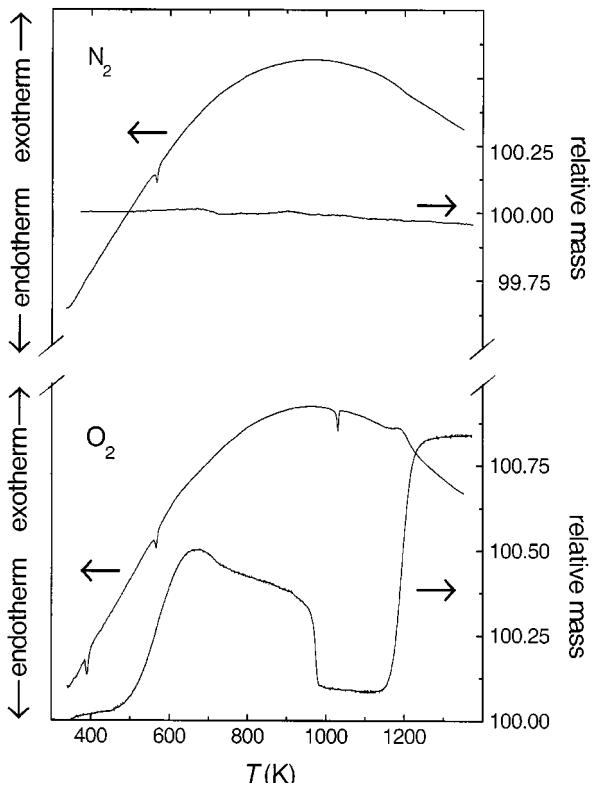

FIG. 1. TGA and DTA data for $Nd_4Co_3O_{10.00}$ measured in nitrogen and oxygen atmospheres, 350–1375 K. Heating rate, $10\ K \cdot min^{-1}$.

Governed by the improved resolution and counting statistics, the synchrotron powder X-ray diffraction pattern for $Nd_4Co_3O_{10.20}$ clearly revealed a systematic splitting of the orthorhombic reflections of the types ($h0l$) and (hkl), indicating a monoclinic deformation, Fig. 2. The diffraction pattern can be indexed on a monoclinic unit cell with space group $C2/m$ as earlier reported for $La_4Co_3O_{10+\delta}$ (8). However, for $Nd_4Co_3O_{10.00}$ and $Nd_4Ni_3O_{9.85}$, the powder neutron diffraction patterns reveal additional reflections that violate the extinction conditions defined by C-centering. The crystal structures for $Nd_4Co_3O_{10+\delta}$ and $Nd_4Ni_3O_{10-\delta}$ were hence described in the monoclinic space group $P2_1/a$ with 18 nonequivalent atoms in the asymmetric unit, in accordance with the recent structure model for $La_4Co_3O_{10+\delta}$ (9). The atomic coordinates were refined after introducing soft constraints for the Co–O and Ni–O interatomic distances.

During the initial refinement of the PND data for $Nd_4Co_3O_{10.00}$, the Co–O distances were restrained to 195.00 ± 0.02 pm, and the soft constraint weight was set to $F = 1000$ (20). The refinement converged satisfactorily, giving R_p(PND) = 3.8%, R_{wp}(PND) = 4.9%, and χ^2(PND) = 1.60. The derived Co–O distances for the corner-sharing octahedra were in the range 193–199 pm. However, relaxation of the soft constraint weight to $F = 1$ gave slightly

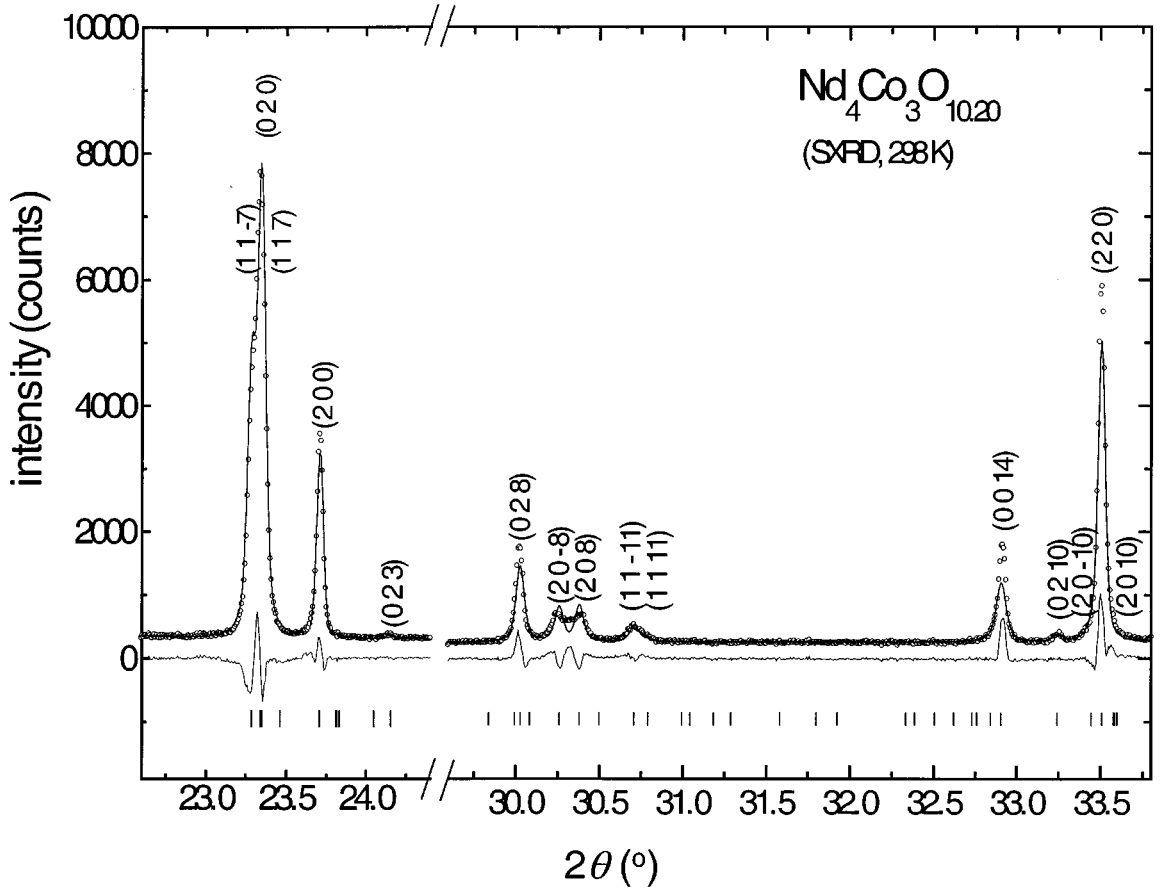

FIG. 2. Selected parts of the SXRD intensity profiles for $Nd_4Co_3O_{10.20}$ at 298 K ($\lambda = 110.103$ pm): observed points (open circles), calculated profiles (full line), difference plot (lower full line), and positions for reflections (vertical bars).

improved reliability factors [R_p(PND) = 3.6%, R_{wp}(PND) = 4.5%, and χ^2(PND) = 1.35] and Co–O distances in the range 190–206 pm. Owing to the slightly improved fit and a reduced spread in the O–Co–O bond angles for the corner-sharing octahedra, the latter model was preferred. The atomic coordinates from the PND data refinements ($F = 1$) were entered thereafter as the starting model in the refinement of the SXRD data. Since oxygen is a weak X-ray scatterer compared to Co and Nd, the atomic coordinates for the oxygen atoms were not refined, and the excess oxygen content ($\delta = 0.20$) was not taken into account. The results from the Rietveld-type refinements ($F = 1$) of the PND and the SXRD data are given in Tables 2, 3, and 4. In Fig. 2 selected parts of the SXRD profiles are shown.

TABLE 2
Crystal Structure Data for $Nd_4Co_3O_{10+\delta}$ and $Nd_4Ni_3O_{9.85}$, Space group $P2_1/a$, $Z = 4$

	$Nd_4Ni_3O_{9.85}$ (PND, 298 K)	$Nd_4Co_3O_{10.00}$ (PND, 298 K)	$Nd_4Co_3O_{10.20}$ (SXRD, 298 K)	$Nd_4Co_3O_{10.00}$ (PND, 8 K)
a (pm)	536.75(2)	536.24(2)	536.39(2)	535.39(3)
b (pm)	545.48(2)	544.51(2)	544.75(2)	543.85(2)
c (pm)	2743.3(1)	2723.8(1)	2722.9(1)	2719.1(1)
β (°)	90.312(2)	90.288(4)	90.229(1)	90.254(4)
V (10^8 pm^3)	8.0320(8)	7.9531(7)	7.9562(9)	7.9171(8)
R_p (%)	3.4	3.6	5.8	3.9
R_{wp} (%)	4.3	4.5	8.0	5.0
χ^2	1.71	1.35	3.23	1.99

Note. Calculated standard deviations are given in parentheses.

TABLE 3
Fractional Atomic Coordinates for $Nd_4Co_3O_{10+\delta}$, 298 K, $\delta = 0.00$ (PND), and $\delta = 0.20$ (SXRD, in Italics)

Atom	Wückoff site[a]	Coordinates		
		x	*y*	*z*
Nd1	4 *e*	− 0.004(2)	0.022(2)	0.2997(5)
		− 0.023(1)	*0.011(3)*	*0.3001(3)*
Nd2	4 *e*	0.495(2)	0.011(2)	0.8011(5)
		0.506(1)	*0.008(3)*	*0.8003(3)*
Nd3	4 *e*	0.030(2)	0.018(2)	0.4312(4)
		0.028(1)	*0.004(2)*	*0.4317(5)*
Nd4	4 *e*	0.525(2)	− 0.005(2)	0.9332(4)
		0.524(1)	*− 0.004(3)*	*0.9324(5)*
Co1	2 *b*	0	1/2	1/2
		0	*1/2*	*1/2*
Co2	2 *a*	0	0	0
		0	*0*	*0*
Co3	4 *e*	0.000(4)	− 0.004(3)	0.1422(5)
		− 0.003(2)	*− 0.002(4)*	*0.1417(5)*
Co4	4 *e*	0.487(4)	0.004(3)	0.6412(5)
		0.482(3)	*0.006(4)*	*0.6397(6)*
O1	4 *e*	0.284(3)	0.285(3)	0.4901(6)
O2	4 *e*	0.297(3)	0.201(3)	0.9910(7)
O3	4 *e*	0.011(3)	0.078(3)	0.0709(4)
O4	4 *e*	0.499(3)	0.066(3)	0.5704(4)
O5	4 *e*	0.257(3)	0.247(3)	0.1496(5)
O6	4 *e*	0.741(3)	0.254(4)	0.6543(5)
O7	4 *e*	0.019(2)	− 0.065(2)	0.2164(4)
O8	4 *e*	0.473(2)	− 0.041(3)	0.7146(4)
O9	4 *e*	0.751(3)	0.247(3)	0.8680(6)
O10	4 *e*	0.275(3)	0.261(3)	0.3669(6)

Note. Space group $P2_1/a$. Calculated standard deviations are given in parentheses. Isotropic displacement factors (in 10^4 pm^2) from PND, $B_{iso}(Nd) = 1.018$, $B_{iso}(Co) = 1.461$, $B_{iso}(O) = 1.624$, and from SXRD, $B_{iso}(Nd) = 3.015$, $B_{iso}(Co) = 1.958$, $B_{iso}(O) = 2.201$. [a] $2a(0,0,0)$, $2b(0,\frac{1}{2},\frac{1}{2})$, $4e(x,y,z)$

Observed, calculated, and difference intensity profiles for the PND data are shown in Fig. 3. The atomic coordinates derived from the SXRD and PND data for the heavy atoms in $Nd_4Co_3O_{10+\delta}$ are equal within one calculated standard deviation, except for *x* and *y* for Nd1, *x* for Nd2, and *y* for Nd3. The slight differences may result from different chemical composition for the studied samples, i.e., $\delta = 0.00$ (PND) and $\delta = 0.20$ (SXRD).

The PND pattern for $Nd_4Co_3O_{10.00}$ at 8 K is virtually identical to the data set at 298 K. The Rietveld-type refinements in space group $P2_1/a$ converged satisfactorily (Table 2), giving $R_p(PND) = 3.9\%$, $R_{wp}(PND) = 5.0\%$, and $\chi^2(PND) = 1.99$. There is no indication for any low-temperature structural deformations for $Nd_4Co_3O_{10.00}$, polymorphism, or long-range magnetic order. For comparison Hansteen *et al.* (21) observed two very weak magnetic reflections for $La_3Co_4O_{10+\delta}$ at 1.7 K.

The PND data for $Nd_4Ni_3O_{9.85}$ were refined according to the procedure outlined above, initially with Ni–O distances restrained to 195.00 ± 0.02 pm and a constraint weight, $F = 1000$ (20). No account for the oxygen deficiency was attempted. The refinement converged satisfactorily, giving Ni–O distances for the corner-sharing octahedra in the range 193–197 pm. The reliability factors $R_p(PND) = 5.1\%$, $R_{wp}(PND) = 6.3\%$, and $\chi^2(PND) = 3.36$ are, however, significantly higher than those obtained for $Nd_4Co_3O_{10.00}$ ($F = 1000$). The situation was greatly improved by relaxing the soft constrains weight to $F = 1$: $R_p(PND) = 3.4\%$, $R_{wp}(PND) = 4.3\%$, and $\chi^2(PND) = 1.71$. Two groups of Ni–O distances thereby emerge, one in the range 190–200 pm, the other 212–213 pm. Results from the Rietveld-type refinements are given in Tables 2, 5, and 6. Observed, calculated, and difference intensity profiles for the PND data are shown in Fig. 4.

There is a strong resemblance between the crystal structures of $Nd_4Co_3O_{10+\delta}$ and $Nd_4Ni_3O_{10-\delta}$, and significant

TABLE 4
Selected Interatomic Distances (pm) and Bond Angles (°) for $Nd_4Co_3O_{10.00}$ at 298 K Derived from PND Data

	Distances (pm)		
Nd1–O6	231(2), 241(2)		
Nd1–O7	232(2)		
Nd1–O8	242(2), 255(2), 288(2), 309(2)		
Nd1–O10	248(2), 269(2)		
Nd2–O5	235(2), 239(2)		
Nd2–O7	236(2), 267(2), 281(2), 317(2)		
Nd2–O8	238(2)		
Nd2–O9	261(2), 261(2)		
Nd3–O1	234(2), 256(2), 268(2), 320(2)		
Nd3–O4	246(2), 257(2), 287(2), 299(2)		
Nd3–O6	303(2), 309(2)		
Nd3–O10	252(2), 256(2)		
Nd4–O2	229(2), 251(2), 271(2), 314(2)		
Nd4–O3	228(2), 252(2), 290(2), 318(2)		
Nd4–O5	286(2), 303(2)		
Nd4–O9	255(2), 270(2)		
Co1–O1	194(1) × 2, 195(1) × 2		
Co1–O4	195(1) × 2		
Co2–O2	195(1) × 2, 197(1) × 2		
Co2–O3	198(1) × 2		
Co3–O3	199(2)		
Co3–O5	192(2), 195(2)		
Co3–O7	206(2)		
Co3–O9	190(2), 193(2)		
Co4–O4	196(2)		
Co4–O6	190(2), 196(2)		
Co4–O8	202(2)		
Co4–O10	194(2), 194(2)		
	Angles Co–O–Co (°)		
Co1–O1–Co1	158(1)	Co1–O4–Co4	159(1)
Co2–O2–Co2	154(1)	Co2–O3–Co3	155(1)
Co3–O5–Co3	168(1)	Co3–O9–Co3	163(1)
Co4–O6–Co4	159(1)	Co4–O10–Co4	166(1)

Note. Atom numbers refer to Fig. 5. Calculated standard deviations are given in parentheses.

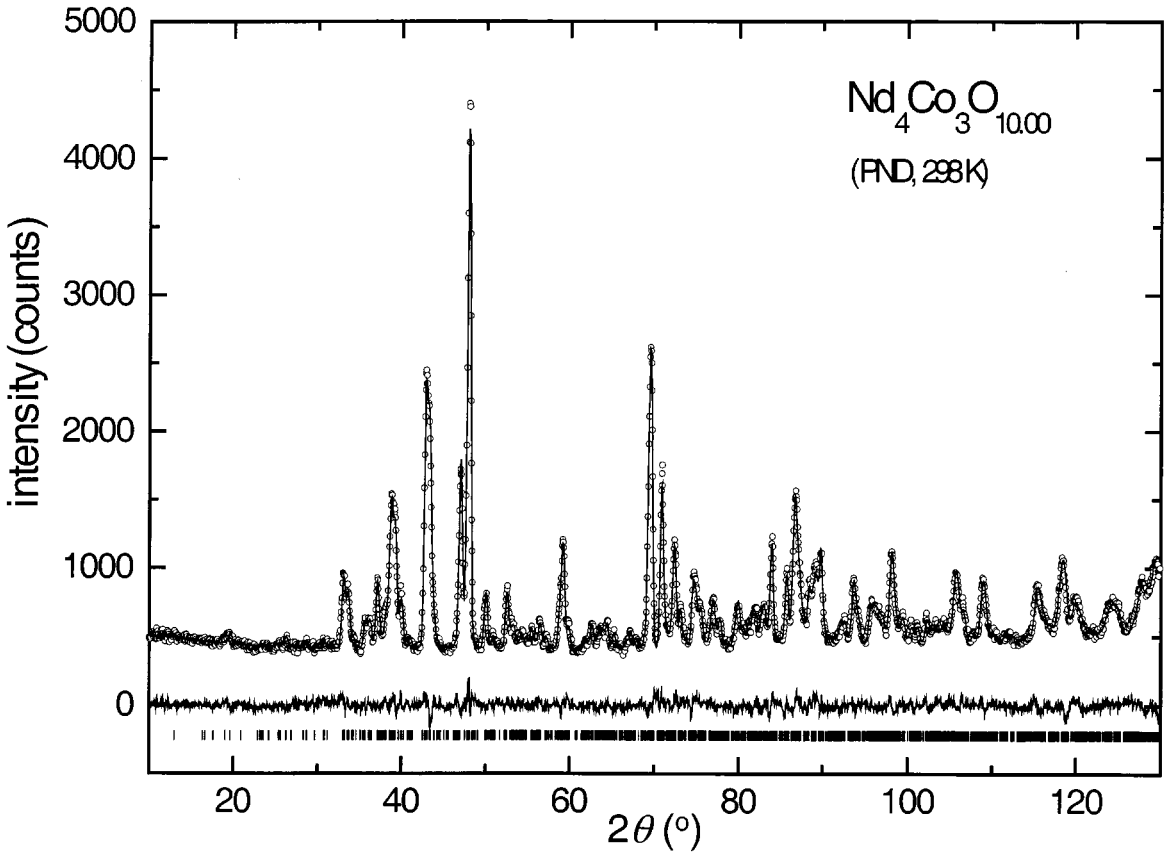

FIG. 3. PND intensity profiles for $Nd_4Co_3O_{10.00}$ at 298 K ($\lambda = 155.58$ pm): observed points (open circles), calculated profiles (full line), difference plot (lower full line), and positions for reflections (vertical bars).

distortions in the MO_6 polyhedra are present. Figure 5 provides a schematic drawing of the crystal structure. The unit cell consists of translated triple perovskite-type layers $(NdMO_3)_3$, M = Co, Ni, characterized by corner-sharing MO_6 octahedra positioned between single NdO layers with NaCl-type atomic arrangement. Within the perovskite layers the Nd atoms have deformed 12-coordination just as in the corresponding $NdMO_3$, M = Co, Ni, (16, 17), whereas the Nd atoms in the NaCl-type layer are 9-coordinated. The Nd–O distances for $Nd_4Co_3O_{10.00}$ and $Nd_4Ni_3O_{9.85}$ are in the range 228–320 pm and 231–326 pm, respectively. The Co–O distances of the corner-sharing octahedra are in the range 190–206 pm, whereas the Ni–O distances are in the range 190–213 pm (Tables 4 and 6). For both $Nd_4Co_3O_{10.00}$ and $Nd_4Ni_3O_{9.85}$ all the long M–O distances are apical in the MO_6 octahedra and point into the NdO layers between the $(NdMO_3)_3$ blocks. The effect is most significant for $Nd_4Ni_3O_{9.85}$ with apical bond lengths 212 (Ni3–O7) and 213 (Ni4–O8) pm. For $Nd_4Co_3O_{10.00}$ the apical Co–O distances are 206 (Co3–O7) and 202 (Co4–O8) pm. The octahedra are tilted and the Co–O–Co and the Ni–O–Ni angles are in the range 154–168°. For comparison the Nd–O distances for $NdCoO_3$ are in the range 230–319 pm and the Co–O–Co angles are 156° (16). The corresponding values for $NdNiO_3$ are 235–319 pm and 157 and 158° (17). The MO_6 octahedra in $Nd_4M_3O_{10}$ (M = Co, Ni) are both tilted and deformed. In particular, the elongation of the M–O distance along [001] for the octahedra next to the NdO layers is much more enhanced for $Nd_4Ni_3O_{10-\delta}$ than for $Nd_4Co_3O_{10+\delta}$. This observation for $Nd_4Ni_3O_{10-\delta}$ may indicate charge ordering, e.g., $Nd_4Ni^{II}Ni^{III}_2O_{10-\delta}$ with Jahn–Teller-deformed Ni(III) in the octahedra having 5 + 1-coordination within the perovskite blocks.

In earlier studies, the deformations and the tilting of the octahedra for the $n = 3$ members of the Ruddlesden–Popper-type series $Ln_{n+1}M_nO_{3n+1}$ could not be resolved owing to the lack of high-resolution PND data (2, 3, 8). However, the presently adopted combination of high-resolution SXRD and PND data facilitates detection of symmetry lowering and description of oxygen displacements connected with tilting of octahedra (9). Long apical Ni–O distances into the LaO layer and tilting of octahedra are also reported for $La_2NiO_{4+\delta}$ (13–15), the $n = 1$ member in the RP-type

TABLE 5
Fractional Atomic Coordinates for $Nd_4Ni_3O_{9.85}$, 298 K (PND)

Atom	Wückoff site[a]	Coordinates		
		x	*y*	*z*
Nd1	4 *e*	− 0.016(2)	0.018(3)	0.3006(5)
Nd2	4 *e*	0.508(2)	0.009(3)	0.8001(5)
Nd3	4 *e*	0.040(1)	0.011(3)	0.4313(5)
Nd4	4 *e*	0.514(2)	− 0.001(3)	0.9316(5)
Ni1	2 *b*	0	1/2	1/2
Ni2	2 *a*	0	0	0
Ni3	4 *e*	− 0.014(2)	0.005(2)	0.1404(3)
Ni4	4 *e*	0.501(2)	0.003(2)	0.6402(3)
O1	4 *e*	0.297(2)	0.300(2)	0.4913(6)
O2	4 *e*	0.267(2)	0.231(3)	0.9891(6)
O3	4 *e*	− 0.003(3)	0.076(4)	0.0690(4)
O4	4 *e*	0.509(3)	0.074(4)	0.5694(4)
O5	4 *e*	0.241(3)	0.242(3)	0.1492(6)
O6	4 *e*	0.758(3)	0.239(3)	0.6516(6)
O7	4 *e*	− 0.031(2)	− 0.051(3)	0.2167(4)
O8	4 *e*	0.525(2)	− 0.061(3)	0.7166(4)
O9	4 *e*	0.753(3)	0.249(3)	0.8715(5)
O10	4 *e*	0.268(3)	0.260(3)	0.3657(4)

Note. Space group $P2_1/a$. Calculated standard deviations are given in parentheses. Isotropic displacement factors (in 10^4 pm^2) from PND, $B_{iso}(Nd) = 0.416$, $B_{iso}(Co) = 0.851$, $B_{iso}(O) = 0.903$. [a] $2a(0,0,0)$, $2b(0,\frac{1}{2},\frac{1}{2})$, $4e(x,y,z)$.

series of $La_{n+1}Ni_nO_{3n+1}$. For $La_2NiO_{4+\delta}$, Brown (22) has modeled the phase diagram as well as various possible structures by means of bond valence considerations. According to Brown (22) the different phases ($La_2NiO_{4+\delta}$) are stabilized at specified pT conditions by certain relaxation mechanisms, such as tilting of the octahedra, increasing of Ni–O distances, and incorporation of excess (interstitial) oxygen in the structure.

Magnetic Properties

Inverse magnetic susceptibility [$\chi_m^{-1}(T)$] data for $Nd_4Co_3O_{10.00}$ in the temperature region from 5 to 920 K are shown in Fig. 6. At low temperatures two effects are evident. The bending of $\chi_m^{-1}(T)$ below $\sim$60 K is probably caused by redistribution between different electronic states for the Nd^{3+} species ($4f^3$), whereas the cusp in $\chi_m(T)$ around 15 K (inset of Fig. 6) reflects probably onset of antiferromagnetic order for the Co sublattice. Long-range magnetic ordering could not be confirmed by PND at 8 K. However, it is probable that lack of additional reflections just reflects low magnetic moments. For comparison the PND data (D1B at ILL) for the analogous $La_4Co_3O_{10+\delta}$ showed that the weak magnetic scattering according to the AF ordering disappeared around 15 K, coincident within the peak in the magnetic susceptibility (21).

In the temperature intervals 60–560 K and from 650–920 K, paramagnetic Curie–Weiss behavior is observed. The anomalous $\chi_m^{-1}(T)$ behavior in the intermediate temperature range 560–650 K resembles that observed for $LaCoO_3$ and $La_4Co_3O_{10}$, and is probably related to temperature-induced spin transitions for Co (8).

Thermal Analysis, Oxygen Content, and Phase Relations

Figure 1 presents thermogravimetric and differential thermal analysis data for $Nd_4Co_3O_{10.00}$ in oxygen and nitrogen atmospheres for the temperature interval 350–1375 K. The TGA data ($pO_2 = 1$ atm) for $Nd_4Co_3O_{10.00}$ show that it oxidizes easily between 450 and 650 K and yields $Nd_4Co_3O_{10.30}$ as the most oxygen rich composition. However, the oxygen content decreases rather smoothly on further heating until about 960 K, where a sudden reduction in

TABLE 6
Selected Interatomic Distances (pm) and Bond Angles (°) for $Nd_4Ni_3O_{9.85}$ at 298 K Derived from PND Data

	Distances (pm)		
Nd1–O6	237(2), 239(2)		
Nd1–O7	233(2)		
Nd1–O8	235(2), 269(2), 278(2), 318(2)		
Nd1–O10	245(2), 269(2)		
Nd2–O5	237(2), 242(2)		
Nd2–O7	245(2), 261(2), 286(2), 309(2)		
Nd2–O8	233(2)		
Nd2–O9	270(2), 273(2)		
Nd3–O1	235(2), 256(2), 266(2), 326(2)		
Nd3–O4	240(2), 247(2), 298(2), 308(2)		
Nd3–O6	287(2), 313(2)		
Nd3–O10	257(2), 263(2)		
Nd4–O2	242(2), 255(2), 277(2), 303(2)		
Nd4–O3	231(3), 266(2), 277(2), 314(2)		
Nd4–O5	290(2), 295(2)		
Nd4–O9	250(2), 256(2)		
Ni1–O1	195(1) × 2, 198(1) × 2		
Ni1–O4	195(1) × 2		
Ni2–O2	193(1) × 2, 195(1) × 2		
Ni2–O3	194(1) × 2		
Ni3–O3	200(1)		
Ni3–O5	190(2), 192(1)		
Ni3–O7	212(1)		
Ni3–O9	192(2), 200(2)		
Ni4–O4	198(1)		
Ni4–O6	191(2), 195(1)		
Ni4–O8	213(1)		
Ni4–O10	190(1), 196(1)		
	Angles Ni–O–Ni(°)		
Ni1–O1–Ni1	154(1)	Ni1–O4–Ni4	157(1)
Ni2–O2–Ni2	161(1)	Ni2–O3–Ni3	156(1)
Ni3–O5–Ni3	165(1)	Ni3–O9–Ni3	161(1)
Ni4–O6–Ni4	161(1)	Ni4–O10–Ni4	168(1)

Note. Atom numbers refer to Fig. 5. Calculated standard deviations are given in parentheses.

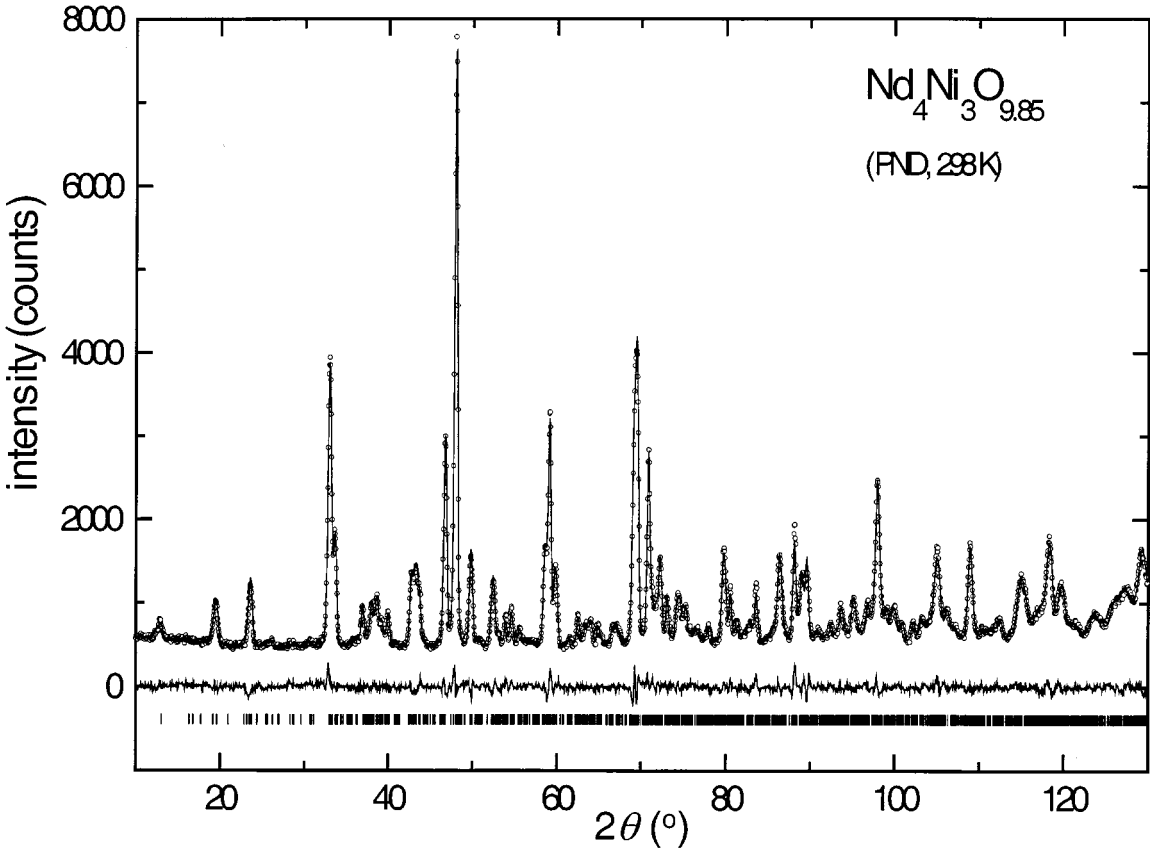

FIG. 4. PND intensity profiles for $Nd_4Ni_3O_{9.85}$ at 298 K ($\lambda = 155.58$ pm): observed points (open circles), calculated profiles (full line), difference plot (lower full line), and positions for reflections (vertical bars).

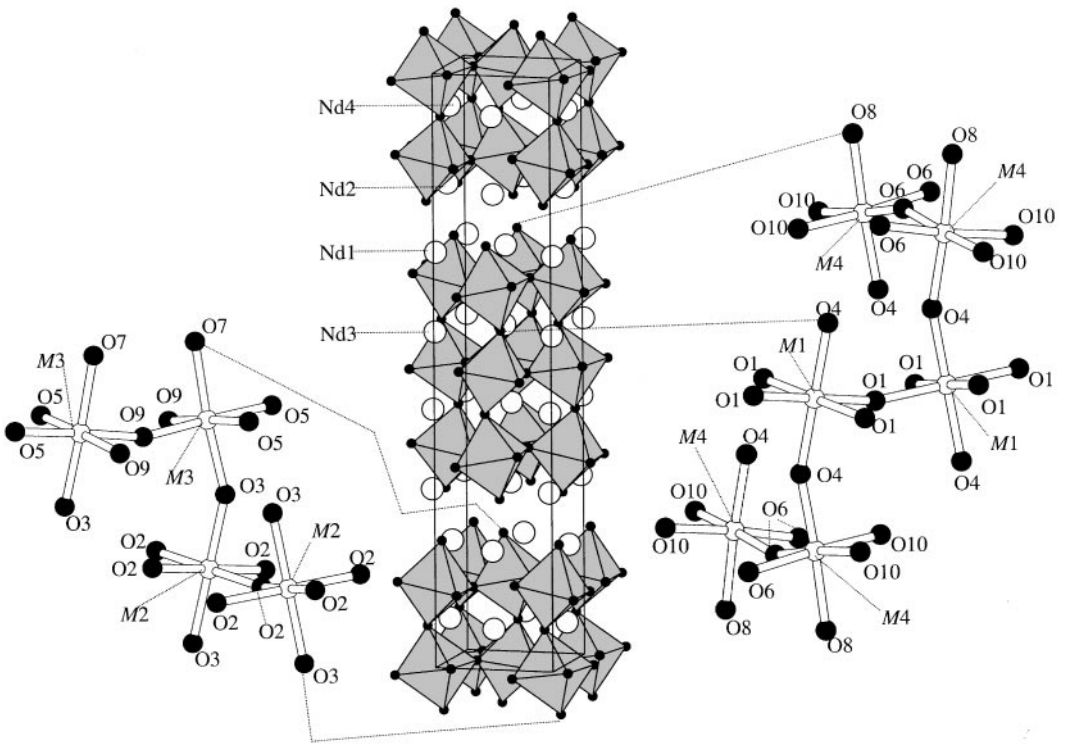

FIG. 5. Schematic representation of the crystal structure for $Nd_4M_3O_{10}$ (M = Co, Ni). Numbering of all O, M and Nd atoms is shown.

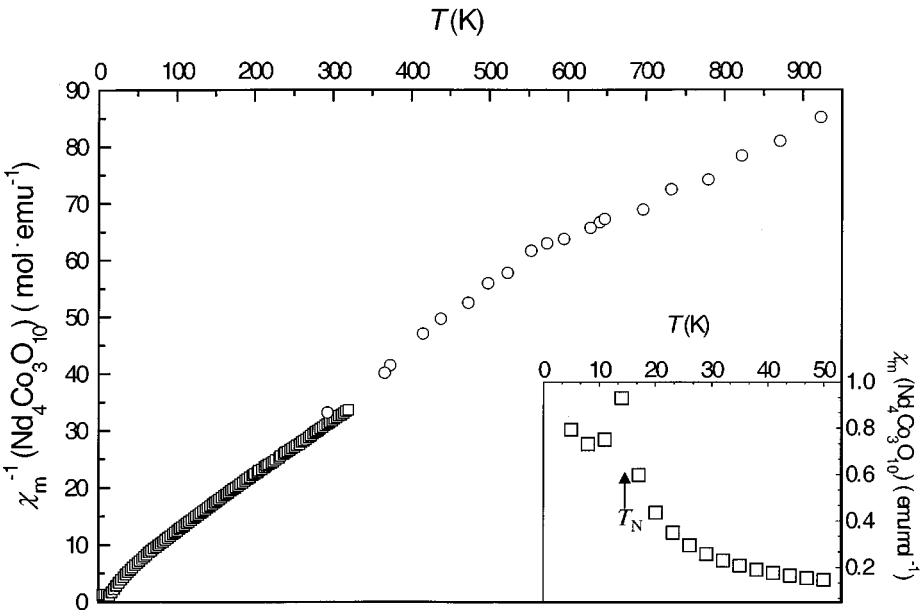

FIG. 6. Inverse molar susceptibility (χ_m^{-1}) for $Nd_4Co_3O_{10.00}$ in the temperature interval 5–925 K. Inset shows molar susceptibility (χ_m) below 50 K.

the oxygen content occurs, and $Nd_4Co_3O_{10.08}$ is obtained. A further slow reduction in the oxygen content is observed, before oxidative decomposition into Nd_2O_3 and $NdCoO_3$ at 1140 K. The TGA data show that the oxygen content for $Nd_4Co_3O_{10.00}$ is essentially unchanged after heating in nitrogen up to approximately 650 K. On further heating a small oxygen mass loss is observed, indicating an oxygen-deficient nonstoichiometry ($\delta < 0.00$).

The DTA data in oxygen reveal three endothermic (390, 560, and 960 K) and one exothermic (1140 K) effect, whereas in nitrogen atmosphere, only one endothermic effect at 560 K is revealed. The endothermic effect at 560 K appears to be independent of composition (cf. TGA data in Fig. 1). It coincides with the change in the slope of $\chi_m^{-1}(T)$ (see Fig. 6), and may hence be electronic in nature.

The endothermic effect at 960 K corresponds roughly in temperature with the sudden mass loss as revealed by TGA. The endothermic effect and the mass jump may indicate the existence of two distinct phases, one being nearly stoichiometric $Nd_4Co_3O_{10+\delta}$ with $\delta \leq 0.08$, the second having a larger oxygen excess, $Nd_4Co_3O_{10+\delta}$ with $0.18 < \delta \leq 0.30$. On the other side, as pointed out earlier the conventional XRD data taken at 298 K for $Nd_4Co_3O_{10.00}$ and $Nd_4Co_3O_{10.20}$ are very similar. For $La_2NiO_{4+\delta}$ a complex situation with the existence of closely related phases with small differences in oxygen content is described (11, 12). One may speculate whether a similar two-phase situation exists for $Nd_4Co_3O_{10+\delta}$. However, this requires more detailed investigations.

The exothermic effect at 1140 K corresponds to oxidation of $Nd_4Co_3O_{10.08}$ into Nd_2O_3 and $NdCoO_3$. At present, the explanation for the endothermic effect at 390 K remains open.

ACKNOWLEDGMENTS

The skillful assistance from the project team at the Swiss-Norwegian Beam Line, ESRF, is gratefully acknowledged.

REFERENCES

1. S. N. Ruddlesden and P. Popper, *Acta Crystallogr.* **11,** 54 (1958).
2. M. Seppänen and M. H. Tikkanen, *Acta Chem. Scand. A* **30,** 389 (1976).
3. M. Seppänen, *Scand. J. Metall.* **8,** 191 (1979).
4. K. Kitayama, *J. Solid State Chem.* **76,** 241 (1988).
5. K. Kitayama, *J. Solid State Chem.* **77,** 366 (1988).
6. Z. Zhang and M. Greenblatt, *J. Solid State Chem.* **117,** 236 (1995).
7. M. D. Carvalho, F. M. A. Costa, I. da Silva Pereira, A. Wattiaux, J. M. Bassat, J. C. Grenier, and M. Pouchard, *J. Mater. Chem.* **7,** 2107 (1997).
8. O. H. Hansteen and H. Fjellvåg, *J. Solid State Chem.* **141,** 212 (1998).
9. H. Fjellvåg, O. H. Hansteen, B. C. Hauback, and P. Fischer, *J. Mater. Chem.*, in press.
10. A. Hayashi, H. Tamura, and Y. Ueda, *Physica C* **216,** 77 (1993).
11. H. Tamura, A. Hayashi, and Y. Ueda, *Physica C* **216,** 83 (1993).
12. H. Tamura, A. Hayashi, and Y. Ueda, *Physica C* **258,** 61 (1996).
13. J. D. Jørgensen, B. Dabrowski, S. Pei, D. R. Richards, and D. G. Hinks, *Phys. Rev. B* **40,** 2187 (1989).
14. J. Rodriguez-Carvajal, M. T. Fernández-Diaz, and J. L. Martinez, *J. Phys. Condens. Matter.* **3,** 3215 (1991).

15. A. Demourgues, F. Weill, B. Darriet, A. Wattiaux, J. C. Grenier, P. Gravereau, and M. Pouchard, *J. Solid State Chem.* **106,** 317 (1993).
16. H. Taguchi, *J. Solid State Chem.* **122,** 297 (1996).
17. J. L. Garcia-Munoz, J. Rodriguez-Carvajal, P. Lacorre, and J. B. Torrance, *Phys. Rev. B* **46,** 4414 (1992).
18. M. C. Morris, H. F. McMurdie, E. H. Evans, B. Paretzkin, J. H. de Groot, C. R. Hubbard, and S. J. Carmel, *Natl. Bur. Stand.* (*U.S*) Monogr. 25, **13,** 35 (1976).
19. N. O. Ersson, Program CELLKANT, Chemical Institute, University of Uppsala, Sweden, 1981.
20. A. C. Larson and R. B. von Dreele, Program GSAS, General Structure Analysis System, LANSCE, MS-H 805, Los Alamos National Laboratory, Los Alamos, NM 87545.
21. O. H. Hansteen, H. Fjellvåg, B. C. Hauback, and P. Fischer, unpublished results.
22. I. D. Brown, *Z. Kristallogr.* **199,** 255 (1992).